

Physics and Computation of Aero-Optics

MENG WANG

Department of Aerospace and Mechanical Engineering, University of Notre Dame, Notre Dame, IN 46556; email: m.wang@nd.edu

ALI MANI

Department of Chemical Engineering, Massachusetts Institute of Technology, Cambridge, MA 02139; email: alimani@mit.edu

STANISLAV GORDEYEV

Department of Aerospace and Mechanical Engineering, University of Notre Dame, Notre Dame, IN 46556; email: sgordeye@nd.edu

Key Words wavefront distortion, turbulent flow, high-fidelity simulation, optical mitigation

Abstract

This article provides a critical review of aero-optics with an emphasis on recent developments in computational predictions and the physical mechanisms of flow-induced optical distortions. Following a brief introduction of the fundamental theory and key concepts, computational techniques for aberrating flow fields and optical propagation are discussed along with a brief survey

of wavefront sensors used in experimental measurements. New physical understanding generated through numerical and experimental investigations are highlighted for a numbers of important aero-optical flows including turbulent boundary layers, separated shear layers and flow over optical turrets. Approaches for mitigating aero-optical effects are briefly discussed.

1 INTRODUCTION

Distortions of optical signals by turbulent flow are widely observed in nature and in technological applications. The twinkling of stars, or stellar scintillation, is the result of refraction of light (electro-magnetic waves) by turbulent fluctuations in the Earth's atmosphere. Shadowgraphs and Schlieren are popular flow visualization techniques which exploit the optical distortions to visualize the flow field that produced them. Over the past four decades, much attention has been paid to the aero-optical effects on the performance of airborne laser systems for communication, target tracking and directed-energy weapons. In these systems optical distortions produced by turbulent flows surrounding the projection aperture pose a serious problem, causing beam distortion, jitter and much reduced effective range. The performance of airborne and ground-based imaging systems is likewise impaired by turbulent flows in the vicinity of the viewing aperture.

The direct cause of optical distortions is the density variations in the flow field. For air and many other fluids, the index of refraction is linearly related to the density of the fluid by the Gladstone-Dale relation (Wolfe & Zizzis 1978). When a beam of an initially planar wavefront is transmitted through a variable density field, different parts of the beam propagate at different local speed of light, resulting in distortions of the wavefront. An optical beam emitted from a projection aperture, or received by a viewing aperture, typically transmits/receives through two distinct flow regions: the active turbulence region induced by solid objects

near the optical window, and atmospheric turbulence. The propagation through atmospheric turbulence has been studied extensively (Chernov 1960, Tatarski 1961) and is relatively well understood. Because of the large temporal and spatial scales associated with atmospheric turbulence, its aberrating effects are of low frequency (< 100 Hz) and can be largely corrected using Adaptive-Optic (AO) systems (e.g. Lloyd-Hart 2003, Hardy 1998). In contrast, the turbulent flow induced by solid surfaces near the aperture, which may be comprised of turbulent boundary layers, free shear-layers, wakes, and shock waves for supersonic and transonic flows, is characterized by much smaller turbulence scales. The size of the optically-active flow region is typically thinner than or comparable to the aperture size. Aero-optics, to follow the conventional definition (Gilbert & Otten 1982, Sutton 1985, Jumper & Fitzgerald 2001), is concerned with the aberrating effects of compressible turbulence in this region. Compared to the atmospheric boundary layer, the aero-optical flow generates stronger optical aberrations at smaller scales and higher frequencies, which are beyond the capability of today's AO technology. Mitigation of these aberrations via active and passive flow-control has been actively pursued in recent years (e.g. Gordeyev et al. 2010a, 2010b).

The types of aero-optical distortions and their far-field impact depend on a number of physical and geometric parameters, including the optical wavelength λ , aperture or beam size a , turbulence length scale ℓ of the aberrating field, and distance of propagation L . In crude terms, small-scale turbulence, with eddy sizes less than the optical aperture ($\ell < a$), causes optical scattering, beam spread, and consequent attenuation of intensity, whereas turbulent eddies larger than or comparable in size to the aperture ($\ell \geq a$) are mostly responsible for the unsteady tilt of the beam (beam jitter) (Cassady et al. 1989). In addition, the mean

density gradient in the beam path causes steady wavefront distortions known as lensing effect. The magnitude of wavefront distortions OPD_{rms} (its precise definition will be given later) is generally small in an absolute sense but can be a significant fraction of, or even exceed the optical wavelength. In other words, the optical phase distortion $2\pi OPD_{rms}/\lambda$, which determines the far-field beam quality, can be easily of $O(0.1)$ to $O(1)$. For the same distortion magnitude, the phase distortion of an aberrated beam is inversely proportional to the optical wavelength, making the aero-optics problem particularly acute for short wavelength beams (Jumper & Fitzgerald 2001). This poses a significant impediment to using shorter wavelength laser systems, which are preferable in the absence of aero-optical aberrations; for an unaberrated beam the diffraction-limited optical intensity scales with $a^2/(L^2\lambda^2)$ (Born & Wolf 2002).

A number of review articles have been written on aero-optics in the past. Research in the pre-1980 era is documented in Gilbert & Otten (1982). Progress since then has been surveyed by Sutton (1985), Jumper & Fitzgerald (2001), and more recently Gordeyev & Jumper (2010) with a focus on the aero-optics of turrets. Among recent advances in this field are high-speed and high-resolution wavefront sensors which allow measurements of instantaneous wavefront errors in unprecedented detail, and the increasing role played by numerical simulations. Application of computational fluid dynamics (CFD) to aero-optics problems has historically lagged most other areas because of the challenging nature of the computations, which must be time-accurate, compressible, and capture optically important flow scales. However, this has begun to change with recent advances in high-fidelity simulation tools and the concomitant increase in computing power. A new generation of computational techniques including direct

numerical simulation (DNS), large-eddy simulation (LES), and hybrid methods combining LES with Reynolds-averaged Navier-Stokes (RANS) approaches, have been employed hand-in-hand with experimental and theoretical approaches to elucidate the physics of aero-optics, predict aberration effects, and develop techniques for their mitigation. This article is an attempt to provide a critical review of some recent progress in the understanding and prediction of aero-optical effects. The discussion is primarily from a computational perspective, although important experimental findings are also included.

2 THEORETICAL BACKGROUND

2.1 Basic Equations

The theoretical foundation for electromagnetic wave propagation in a turbulent medium is discussed extensively in Monin & Yaglom (1975), and is briefly outlined here in the context of aero-optics. In the most general sense, the propagation of electromagnetic waves is governed by the Maxwell equations along with compressible Navier-Stokes equations. Various simplifications can be made depending on relevant physical parameters and length and time scales. For aero-optical problems, the time scale for optical propagation is negligibly short relative to flow time scales, and hence optical propagation can be solved in a frozen flow field at each time instant. If the optical wavelength is much shorter than the smallest flow scale (Kolmogorov scale), which is generally the case, the effect of depolarization is negligible, and the Maxwell equations reduce to a vector wave equation in which all three components of the electromagnetic field are decoupled. A scalar

component of the electric field at frequency ω is governed by

$$\nabla^2 U + \frac{\omega^2 n^2}{c_0^2} U = 0, \quad (1)$$

where c_0 is the speed of light in vacuum and n is the index of refraction. The latter is related to the density of air via the Gladstone-Dale relation: $n(x, y, z) = 1 + K_{GD}(\lambda)\rho(x, y, z)$, where K_{GD} is the Gladstone-Dale constant and is in general weakly dependent on the optical wavelength (Wolfe & Zizzis 1978). In aero-optics, fluctuations in index of refraction are small ($\sim 10^{-4}$) and have scales much larger than the optical wavelength, and hence an optical beam propagates predominantly in the axial (z) direction with slowly varying amplitude. It is customary to invoke the paraxial approximation, which assumes $U(x, y, z) = A(x, y, z) \exp(-ikz)$ and $|\partial^2 A / \partial z^2| \ll |k \partial A / \partial z|$, where $k = \omega / c_\infty$ is the optical wavenumber in the free stream. This leads to the parabolized wave equation for the complex amplitude

$$-2ik \frac{\partial A}{\partial z} + \nabla_\perp^2 A + k^2 \left(\frac{n^2}{n_\infty^2} - 1 \right) A = 0, \quad (2)$$

where ∇_\perp^2 is the Laplacian operator in the transverse directions. Effects not included in the paraxial wave equation include large-angle scattering and energy dissipation/absorption, which are insignificant for aero-optical problems. A detailed discussion of the approximations and limitation of applicability is given by Monin & Yaglom (1975).

Further approximations can be made to obtain closed-form solutions to Equation 2. As depicted schematically in Figure 1, the propagation domain consists of two distinct regions: the optically active turbulent near-field (from $z = 0$ to z_1) and the free space extending to the distant far field (from $z = z_1$ to L , with $L \gg z_1$). For transmission across the aero-optical region, it can be shown that the

contribution from the Laplacian term in Equation 2, which represents the diffraction effect, is negligible relative to the last term for $z_1 \ll \ell_\perp^2/\lambda$, where ℓ_\perp is the transverse length scale of the optical wave. If the refractive index is expressed as $n = n_\infty + n'$, and the linear approximation $n^2/n_\infty^2 \approx 1 + 2n'/n_\infty$ is made about the index-of-refraction deviation from the free-stream value, Equation 2 can be integrated from 0 to z_1 to obtain $A(x, y, z_1) = A(x, y, 0) \exp\left(-\frac{ik}{n_\infty} \int_0^{z_1} n'(x, y, z) dz\right)$, or

$$U(x, y, z_1) = U(x, y, 0) \exp\left(-ik_0 \int_0^{z_1} n(x, y, z) dz\right), \quad (3)$$

where $k_0 = k/n_\infty = \omega/c_0 = 2\pi/\lambda_0$ is the optical wavenumber in vacuum.

Once the solution past the aero-optical region, $U(x, y, z_1)$, has been determined, it can be used as the initial condition to propagate the optical beam to the far field using the wave equation (Equation 1) or paraxial wave equation (Equation 2). By setting $n = n_\infty$ and $n' = 0$, either equation can be solved analytically using Fourier transform techniques, which are the basis for Fourier optics (Goodman 2004).

2.2 Near-Field Distortion Measures

Equation 3 suggests that the dominant aero-optical effect after transmission through the turbulence region is a phase distortion of the optical wavefront; the amplitude is approximately unchanged. The integral in Equation 3 is known as the optical path length (OPL). It is most commonly derived from geometric optics by assuming straight ray paths and is generally dependent on the flow-time scale (but not optical time scale):

$$\text{OPL}(x, y, t) = \int_0^{z_1} n(x, y, z, t) dz. \quad (4)$$

Ray bending can be accounted for by solving the eikonal equation (Born & Wolf 2002) but is generally negligible for aero-optics. In practice, the relative difference in the OPL over the aperture is a more relevant representation of wavefront distortions. It is called the optical path difference (OPD) and is defined as

$$\text{OPD}(x, y, t) = \text{OPL}(x, y, t) - \langle \text{OPL}(x, y, t) \rangle, \quad (5)$$

where the angle brackets denote spatial averaging over the aperture. The optical phase distortion is then $2\pi\text{OPD}/\lambda$. It should be noted that the optical wavefront, defined as the locus of constant phase, is (after removing the spatial mean) the conjugate (negative) of the OPD: $W(x, y, t) = -\text{OPD}(x, y, t)$.

To facilitate analysis and mitigation of distortions, the time-dependent OPD is often decomposed into a time-averaged spatial component, called the steady-lensing term, $\text{OPD}_{\text{steady}}(x, y)$, and an unsteady component. The unsteady part can be further split into a spatially linear component, called unsteady tilt or beam jitter, and the rest, usually called high-order distortions (Gordeyev & Jumper 2010). In other words,

$$\text{OPD}(x, y, t) = \text{OPD}_{\text{steady}}(x, y) + [A(t)x + B(t)y] + \text{OPD}_{\text{high-order}}(x, y, t). \quad (6)$$

Physically, these three components affect an outgoing beam in different ways. The steady-lensing term, $\text{OPD}_{\text{steady}}(x, y)$, is a function of the time-averaged density field only and imposes a steady distortion like defocus, coma and so on. The tilt or jitter, represented by the second term on the right-hand side, does not change the spatial distribution of the outgoing beam but simply re-directs it in directions defined by functions $A(t)$ and $B(t)$. The specific forms of $A(t)$ and $B(t)$ depend on the definition of tilt. For the so-called *G*-tilt (Tyson 2000), $A(t)$ and $B(t)$ are the spatially-average gradient components of the OPD in x - and y -directions,

respectively, whereas for the Z -tilt (Sasiela 2007), they are defined such that the magnitude of $\text{OPD}_{\text{high-order}}$ in Equation 6 is minimized in the least square sense at each time instant. Finally, the high-order term causes the beam to change its shape and intensity distribution.

The decomposition in Equation 6 is particularly useful when an adaptive optic system is used to correct for aberrating wavefronts. The purpose of an adaptive optic system is to apply a conjugate wavefront to the outgoing beam so that it will negate optical aberrations from the flow and the beam will become re-collimated after passing through the turbulent media (Tyson 1997). Among the distortion components given in Equation 6, steady lensing is easily corrected by a deformable mirror with a large range of motion, the tilt component is removed using a fast-steering mirror, and the high-order term can be compensated for by using a high-bandwidth deformable mirror (Tyson 1997).

2.3 Statistical Theory

An important equation relating the statistical properties of a turbulent medium and those of aero-optical aberrations, the so-called linking equation, was derived by Sutton (1969) (see also Sutton 1985, Steinmetz 1982, and Havener 1992). In the most general form, the linking equation can be written as,

$$\overline{\langle \text{OPD}^2 \rangle} = K_{GD}^2 \int_0^{z_1} \int_0^{z_1} \text{Cov}_{\rho'}(z, z') dz' dz, \quad (7)$$

where the overbar denotes time averaging, $\text{Cov}_{\rho'}$ is the covariance function of density fluctuations, and z_1 is the integration distance along the traversing beam through the turbulence region. In the case of homogeneous turbulent flows, the density covariance is most commonly modeled by an exponential function (Steinmetz 1982), $\rho_{rms}^2 \exp(-|z - z'|/\Lambda)$, or a Gaussian function (Wolters 1973),

$\rho_{rms}^2 \exp(-|z - z'|^2 / \Lambda^2)$, where Λ is the characteristic length scale for density fluctuations. Substituting these models into Equation 7 leads to

$$\overline{\langle \text{OPD}^2 \rangle} = \alpha K_{GD}^2 \int_0^{z_1} \rho_{rms}^2(z) \Lambda(z) dz, \quad (8)$$

where $\alpha = 2$ for the exponential covariance function and $\sqrt{\pi}$ for the Gaussian covariance function. Both the density fluctuation magnitude and length scale are allowed to vary slowly along the beam path.

Both forms of the linking equation allow one to calculate aero-optical distortions indirectly from statistical properties of the turbulent flow. Since the full covariance matrix in Equation 7, is difficult to measure experimentally, the simplified equation, Equation 8 is commonly used instead. However, since the simplified linking equation is derived for homogenous and isotropic turbulent flows, its applicability to inhomogeneous flows, such as shear layers (Hugo & Jumper 2000) and boundary layers (Gilbert & Otten 1982, Tromeur et al. 2006b), has been questioned. It has been shown that with appropriate choice of the length scale Λ_ρ , the simplified linking equation can be used to obtain accurate results for flow fields with anisotropic and inhomogeneous turbulence. The key is to use the correct density correlation length defined based on Equation 7 (Wang & Wang 2011).

3 PREDICTION OF FAR-FIELD DISTORTIONS

Given the OPD profiles after the beam passes the turbulence region, its free-space propagation from $z = z_1$ to L can be solved using Fourier optics to obtain the exact far-field projection. Figure 2 shows an example of instantaneous far-field irradiance of a Gaussian beam subject to strong aero-optical distortions by the turbulent wake behind a circular cylinder of diameter D (Mani et al. 2009). It

contrasts the distorted beam pattern to that of an undistorted, diffraction limited beam for two different optical wavelengths. In this case the near-field OPD_{rms} is $6.7 \times 10^{-6}D$, corresponding to phase distortions of $2\pi\text{OPD}_{rms}/\lambda \approx 17$ and 4.2 for the two wavelengths (6.7 and 1.7 respectively, after tilt removal). Drastic losses of far-field beam intensity and coherence are observed. Note that in the absence of distortions, the shorter wavelength beam delivers more energy to the target than the longer wavelength one, but this advantage is offset by aero-optical distortions. In fact, the ratio of the maximum intensity of the distorted beam to that of the undistorted one is about 1.5% for the shorter wavelength case and 10% for the longer wavelength case.

While Fourier optics provides a complete description of the optical propagation, it requires as input detailed spatio-temporal history of the near-field wavefront, which may not be available from experimental measurements. Furthermore, from a systems point of view, statistical measures, rather than instantaneous quantities, are of primary interest, and it is desirable to relate the far-field beam statistics to statistics of the aberrating flow field. A widely-adopted relation is the Maréchal approximation (Maréchal 1947, Born & Wolf 2002) for the Strehl ratio (SR), defined as the ratio of the peak on-axis far-field irradiance of an aberrated beam (after tilt removal) to the corresponding peak irradiance of an unaberrated beam; it is a measure of beam quality relative to a diffraction-limited beam at each time instant. In his original paper Maréchal (1947) showed that, in the limit of small phase distortions, $\text{OPD}_{rms}/\lambda < 0.1$, $\text{SR}(t) = I(t)/I_0 \approx 1 - [2\pi\text{OPD}_{rms}(t)/\lambda]^2$. A more commonly adopted expression, however, takes the exponential form

$$\frac{I(t)}{I_0} = \text{SR}(t) \approx \exp \left[- \left(\frac{2\pi\text{OPD}_{rms}(t)}{\lambda} \right)^2 \right]. \quad (9)$$

This equation, also known as Maréchal approximation, was proposed by Mahajan

(1982, 1983) based on empirical fitting of SR versus OPD_{rms} data for a variety of distortion modes. In comparison with the original form, Mahajan found that Equation 9 gave a better approximation for the Strehl ratio over a wider range of phase distortions.

Ross (2009) recently re-examined the derivation of the Maréchal approximation and found that for OPD data with Gaussian probability-density distribution, Equation 9 was in fact exact. It is important to note that the original Maréchal approximation is a relationship between the spatial statistics of the instantaneous wavefront and the far-field intensity. In the case when the aperture size is much larger than the turbulence length scale, $a \gg l$, Steinmetz (1982) showed that the Maréchal approximation is also approximately valid for the time-averaged Strehl ratio:

$$\overline{SR} \approx \exp \left[- \left(\frac{2\pi OPD_{rms}}{\lambda} \right)^2 \right]. \quad (10)$$

This equation is known interchangeably as the large-aperture approximation and Maréchal approximation. However, in many practical applications, the assumptions of large (infinite) aperture and small aberrations are not exactly valid. For stationary, Gaussian-in-space processes, an exact version of time-averaged Maréchal approximation can be expressed in terms of the temporal probability-density function of OPD_{rms} (Porter et al. 2011).

The time-averaged version of Maréchal approximation is currently the *de facto* standard approach for estimating and comparing the effect of aero-optical distortions on the degradation of beam performance. Despite its routine use, some uncertainties still exist concerning the accuracy and applicability of this approximation, particularly for cases with large phase distortions.

Mani et al. (2006) proposed a new set of statistical measures to quantify the

far-field optical distortions, and derived exact algebraic relations between these measures and the statistics of near-field OPD. Instead of characterizing beam distortions in terms of peak irradiance, they proposed to use the spatial spread of the beam, in terms of the second spatial moment of the far-field irradiance, as a measure of distortion (see Figure 2). Through statistical solutions of the paraxial wave equation, it was shown that the square of the beam spread about its center (i.e. with tilt removal) can be expressed, in the Fraunhofer limit $L\lambda/a^2 \gg 1$, as

$$\left(\frac{\sigma_x}{L}\right)^2 = C \frac{\lambda^2}{\pi^2 a^2} + \left\langle \left(\frac{\partial}{\partial x} \text{OPD}\right)^2 \right\rangle. \quad (11)$$

where σ_x is the beam spread in the x -direction, a is the aperture diameter, the prime represents deviation from the mean value, and the angle brackets indicate a spatial average. C is a constant determined by the shape of the aperture and its optical intensity profile; it is an $O(1)$ quantity for beams with smooth aperture intensity profiles and is exactly equal to one for Gaussian beams. The beam spread in the y -direction (see Figure 2) has the same form. One can observe clearly that the anisotropy of the beam spread about its axis is directly linked to the anisotropy of OPD gradients and thus in the refractive index field.

The first term on the right-hand side of Equation 11 represents the effect of diffraction on the beam spread, which is decoupled from the aero-optical effect represented by the second term. The latter is simply the variance of OPD gradient. The ratio of these two terms was proposed by Mani et al. (2006) as the basis for a new distortion measure, which they termed the “fidelity ratio”. Compared with the Strehl ratio based on Maréchal approximation, the new measure has the advantage of being applicable to highly aberrated beams because Equation 11 is exact. The disadvantage is that its applicability is limited to beams with initially smooth (continuous) aperture intensity profiles since the beam spread becomes a

singular measure for beams with discontinuous intensity profile. Equation 11 also provides insight into scaling of aero-optical distortions with key optical parameters such as the aperture size. For instance, one can expect that the aero-optical effect is a lesser concern for naked human eyes (with $a \sim 1$ mm) compared to tactical airborne system (with $a \sim 20$ cm), since the far-field resolution of an eye is predominantly limited by the diffraction term for typical aero-optical flows.

4 COMPUTATIONAL AND EXPERIMENTAL APPROACHES

4.1 Computational Methods

4.1.1 OPTICAL PROPAGATION Computations of aero-optics consist of two essential parts: solutions of the aberrating flow field via CFD techniques and propagation of the optical beam through the aberrating flow to the target. In practices, the beam propagation is easily computed by a combination of ray tracing with Fourier optics. For propagation through the thin aero-optical region surrounding an aperture, ray optics is applicable, and Equation 3 or its OPD representation provides satisfactory results. The numerical evaluation involves a simple integration of the index-of-refraction field along the optical path. The validity of this approach is established based on scaling arguments, and has been confirmed numerically by White (2010) through a comparison with the numerical solution of paraxial wave equation (Equation 2) using a high-order scheme in the case of optical propagation through a supersonic turbulent boundary layer. Beyond the aero-optical region, the index of refraction is considered uniform, and propagation in free space can be treated with Fourier optics as exemplified in Section 3. If the target is in the optical far field, the Fraunhofer approximation (Goodman 2004) can be applied to simplify the solution.

The long-range propagation of optical waves in atmospheric turbulence is significantly more difficult to compute. Ray tracing is invalid because amplitude variations accumulated over a large distance are significant, and numerical solutions of the wave equation or paraxial wave equation are impeded by the vast scale disparity and prohibitive computational expenses required to obtain the fluctuating index-of-refraction field over the entire propagation range. Current approaches are predominantly based on statistical modeling of the turbulent media in terms discrete thin “phase screens” along the direction of propagation and numerical integration of the paraxial wave equation (e.g. Coles et al. 1995, Frehlich 2000). Because its distortion effect can be corrected by adaptive optic techniques, atmospheric propagation is not considered a pressing issue in aero-optics and is therefore not discussed further.

4.1.2 COMPUTATION OF ABERRATING FLOWS The most challenging part of computational aero-optics is the computation of the aberrating flows surrounding optical apertures. These flows are compressible, turbulent, generally three-dimensional at high Reynolds numbers and often with separation. In order to accurately compute the index of refraction field, turbulence scales over all optically relevant wavenumbers and frequencies must be captured, which poses a significant challenge in terms of computational expenses and numerical accuracy. Because of these difficulties, application of CFD to aero-optics did not start until late 1980s, and significant growth occurred only in the last decade as a result of the advancement and maturation of high-fidelity simulation techniques.

Limited by computing power, early numerical investigations involved two-dimensional solutions of Euler equations and RANS equations. Cassady et al. (1989) performed RANS simulations of the flow over an open cavity in the Mach

number range between 0.6 and 0.8 under standard conditions at altitudes of 40,000 to 50,000 feet, and analyzed image distortions at different look angles across the shear layer. Because their RANS calculations did not capture the coherent structures in the shear layer, only the steady tilt of the optical beam was predicted directly. Beam jitter was modeled, and high-order distortions were largely unaccounted for. Tsai and Christiansen (1990) solved Euler equations numerically to study the degradation of a laser beam by a plane mixing layer at low Mach numbers ($M_1 = 0.2$ and $M_2 = 0.1$ for the two air streams). Their solutions were able to capture qualitative features of large-scale coherent structures including vortex pairing, but this is a result of the numerical viscosity in the simulation code based on a combination of MacCormack and Godunov methods.

While the Euler and RANS solutions are computationally efficient, their usefulness for aero-optical predictions is limited. Euler equations do not describe the correct physics of refractive-index fluctuations in a turbulent flow and must rely on numerical dissipation to mimic the effect of physical viscosity. In a steady RANS calculation, all turbulence scales are modeled, resulting in an ensemble-averaged (time-averaged) density field from which the steady-lensing effect of optical aberrations can be evaluated but not the unsteady tilt and high-order effects. It is, however, possible to combine a RANS simulation with a statistical model for optics, such as the linking equation, Equation 8, to estimate the aero-optical effects. This provides a practical approach for high-Reynolds-number flows in realistic configurations which is not currently affordable with more accurate techniques. Smith et al. (1990) proposed a transport equation for the variance of index-of-refraction fluctuations, and solved it along with compressible turbulent boundary-layer equations with k - ε model for a plane mixing layer. The

computed refractive-index variance, together with the turbulence length scale estimated based on k and ε solutions, allowed the linking equation to predict the wavefront error for a beam passing the mixing layer and its impact on target intensity. Using the same methodology, Pond & Sutton (2006) performed an aero-optic analysis of a nose-mounted optical turret on an aircraft. Their solutions are based on three-dimensional RANS equations, the k - ε model, and the transport equation for the refractive-index variance proposed by Smith et al. (1990).

For more accurate computations of index-of-refraction fluctuations, a hierarchy of high-fidelity methods including DNS, LES and hybrid RANS/LES approaches, are available. Among them DNS (Moin & Mahesh 1998), which resolves all flow scales down to the dissipative scale, is the most accurate. Due to the well-known Reynolds number limitation it is primarily a research tool and has only found limited use in aero-optics. Truman & Lee (1990) and Truman (1992) used DNS data to investigate the phase distortions in optical beams through a homogeneous shear flow with uniform mean shear and a turbulent channel flow. Their simulations were based on incompressible Navier-Stokes equations, and the fluctuating index-of-refraction field was represented as a passive scalar. The magnitude of phase distortions was found to be sensitive to the direction of propagation, which was explained in terms of the anisotropic vortical structures in the flow. Despite the low Reynolds numbers and incompressible nature of the simulations, the findings in these studies are qualitatively consistent with subsequent experimental measurements (Cress et al. 2008) and results of compressible flow simulations (Wang & Wang 2009); see Section 5.1.

LES offers a less expensive alternative to DNS because it resolves only the

large, energy-containing scales of fluid motions which are optically important. The effect of small scales are modeled by a subgrid-scale (SGS) model. The prevalent SGS models in use today are of the Smagorinsky eddy-viscosity type (Smagorinsky 1963) for which the dynamic procedure (Germano et al. 1991, Lilly 1992, Moin et al. 1991) provides a robust way of computing the model coefficient from the resolved scales, thus eliminating the need for adjustable model parameters. Some practitioners use implicit LES, or ILES, in which a high-order low-pass spatial filter acts as the SGS model to selectively provide numerical dissipation (e.g. Visbal 2009, White et al. 2010), often out of numerical-stability consideration for high-order accurate compressible LES codes.

The first application of LES to aero-optics was made by Childs (1993), who carried out LES of high-speed turbulent mixing layers at convective Mach numbers of up to 2.5 and analyzed the induced wavefront distortions. Significant growth in LES-based investigations occurred in the past decade as a result of maturation of LES methodology, advances in computing power and a renewed interest in the field of aero-optics. LES has to date been employed in a variety of aero-optical configurations including turbulent shear layers (Visbal 2008, Visbal 2009, White et al. 2010), open-cavity flows (Sinha et al. 2004, Visbal 2008), turbulent boundary layers (Tromeur et al. 2003, 2006a, 2006b; Wang & Wang 2009, 2011; White & Visbal 2010), flow over a cylinder (Mani et al. 2009), and flows over cylindrical turrets (Wang & Wang 2009, Morgan & Visbal 2010, Wang et al. 2010) and realistic three-dimensional turrets (Jones & Bender 2001, Arunajatesan & Sinha 2005). In addition, there have been attempts to employ LES to predict the effect of passive flow control on aero-optical mitigation (Morgan & Visbal 2010, Wang et al. 2010). Among the afore-mentioned studies, the simple

canonical flows such as turbulent shear layers, boundary layers and flow over a cylinder were simulated to study the fundamental physics of aero-optics and were afforded adequate grid resolution and numerical accuracy. Some of the findings from these studies will be discussed in Section 5. On the other hand, the simulations of three-dimensional turret flows were under-resolved and used simulation codes with large numerical dissipation.

To further reduce computational costs for wall-bounded flows at high Reynolds numbers, LES can be combined with a RANS model to form a hybrid RANS/LES method. A popular class of hybrid methods, proposed and recently reviewed by Spalart (2009), is detached-eddy simulation (DES). In this method less expensive RANS equations are solved with an appropriate turbulence model in an attached boundary layer, and LES is used to treat the separated-flow region. It therefore avoids the stringent boundary-layer resolution demanded for LES but at the same time inherits many weaknesses of RANS methods such as poor prediction of pressure-driven incipient separation. In addition, the lack of turbulent fluctuations prior to separation may affect the instability of the separated shear layer and its aero-optical behavior. DES and similar hybrid methods have been applied in simulations of flow over three-dimensional optical turrets, with limited success (Nahrstedt et al. 2008, Ladd et al. 2009, Morgan & Visbal 2010); more discussion will follow in Section 5.3. Another class of hybrid methods, which is more accurate and robust but computationally more demanding than DES, is LES with wall modeling (Piomelli & Balaras 2002, Wang & Moin 2002). In this case only the near-wall region in a turbulent boundary layer is treated with RANS modeling, whereas the bulk part of the boundary layer is computed using LES. This avoids the strong Reynolds number scaling of grid-resolution requirements in a

fully resolved LES. LES with wall modeling has to date not been used for aero-optical computations but holds a bright promise as computing power continues to grow.

4.2 Resolution Requirement

Turbulent flows relevant to aero-optics contain eddies over a wide range of scales, typically from order meter to order 10 microns. When practical computational tools such as LES is employed for aero-optical computations it is important to ensure that the optical effects of the unresolved flow is negligible. Addressing this issue requires an understanding of the range of optically active flow scales in aero-optical flows. Such knowledge not only helps select the mesh size for computations, but also provides insight for adaptive optics requirements. In other words, if distortion effects are to be canceled by deformable mirrors, the range of length scales (and frequencies) to be corrected can be determined from the same theory.

From Equation 3 it is clear that lack of flow resolution will cause errors in computation of the optical phase when the beam is traced through the turbulence. If the true refractive-index field is written in terms of the resolved field, n_r , and the error, n_e which is basically the unresolved n , substituting $n = n_r + n_e$ into Equation 3 yields:

$$U(x, y, z_1) \simeq U_r(x, y, z_1) - \left(ik_0 \int_0^{z_1} n_e(x, y, z) dz \right) U_r(x, y, z_1), \quad (12)$$

where a leading order expansion for small n_e is used and U_r is the computed optical wave (by substituting the resolved field, n_r , into Equation 3). According to this description, the true optical wave at z_1 is written in terms of two beams: the first term on the right hand side represents the computed beam and the

second term represents the “error” beam associated with lack of resolution in predicting the refractive index field. An acceptable resolution should ensure that the energy of the error beam is much smaller than the energy of the resolved beam.

Mani et al. (2008) used this criterion in conjunction with the Kolmogorov hypothesis for unresolved turbulence to develop a theory to estimate the smallest optically-important flow length scale in a general aero-optical framework. According to their analysis, in the limit of high Reynolds number the smallest optically important flow scale does not depend on the Kolmogorov scale. For a given geometry, this length scale depends only on the flow Mach number, freestream refractive index n_∞ , and the optical wavelength λ_0 :

$$\ell_c \approx C \frac{\lambda_0^{6/7} \ell^{4/7}}{M^{12/7} (n_\infty - 1)^{6/7} z_1^{3/7}}, \quad (13)$$

where ℓ_c is the smallest optically active scale, M is the turbulent Mach number, z_1 is the depth of the turbulent field in the propagation direction, and ℓ is the length scale of the largest turbulent eddy. The proportionality constant C in Equation 13 can be written in terms of the universal constant of the Kolmogorov spectrum and the acceptable energy threshold for the “error” beam in Equation 12, and is generally of small value; for example, this constant is approximately 0.05 for 95% accuracy (see Mani et al. 2008 for details). A crude estimate based on practical aero-optical parameters indicates that the length scale predicted by this theory is in the inertial range and of order of typical LES resolutions. This indicates that LES, without the need for subgrid optical modeling, is adequate for aero-optical computations, and DNS is not necessary. Extension of this analysis to complex flow regimes with inhomogeneous turbulence and mesh spacing can be found in Mani et al. (2008).

The results of this analysis and the conclusion regarding negligible optical effects by small-scale turbulence are consistent with previous experimental findings of Zubair & Catrakis (2007), who verified the “resolution robustness” of optical distortions by systematically examining the refractive-index data of separated shear layers at various resolution levels.

4.3 Wavefront Sensors

The most critical device for experimental aero-optics is the wavefront sensor. The wavefront is the locus of constant phase for the complex intensity (see Equation 3). This quantity cannot be measured directly, as any light-recording device is sensitive to the absolute value of the complex intensity only. Wavefront sensors can be divided into several categories depending on how the wavefront is measured, which also defines the sensor performance in terms of the dynamic range, temporal and spatial resolution and sensitivity to real-life corrupting effects such as the quality of the optical elements involved or large jitter of the incoming beam due to mechanical vibration. Interferometry-based sensors combine the measured wavefront with a known wavefront, which creates an interference pattern with variable light intensity on the sensor, and the measured wavefront can be directly reconstructed from it. They have very good spatial (tens of thousands of points) and temporal (up to 100 kHz) resolution, but usually require very good optical elements to manipulate the incoming beam before sending it to the sensor. Slope-based sensors, like a Shack-Hartmann sensor (Tyson 1997), rely on the Huygens’ Principle, which states that the wavefront propagates in the direction normal to itself (Born & Wolf 2002). A lenslet array is used to break the wavefront into a large number of small sub-apertures and the overall tilt or the

deflection angle over each sub-aperture is measured by tracing the dot motion at the lenslet focal plane. The deflection angles are gradients of the wavefront, and different techniques are used to reconstruct the original wavefront. These sensors are perhaps the most robust and widely used wavefront sensors with a large dynamic range and relative insensitivity to the quality of the optical components and the overall beam jitter. The spatial resolution is, however, limited by the lenslet array, which typically has several thousand sub-apertures, and temporal resolution is usually limited to several kHz; however, more recent cameras have now increased this limit to tens of kHz. Finally, phase-diversity and distorted-grating sensors use the intensity transport equation to measure the wavefront (Blanchard et al. 2000) and ultimately are sensitive to the wavefront curvature. They have good spatial resolution (several thousand points) and very high temporal resolution (up to 100 kHz), but typically require good optical components to manipulate the beam, as well as small overall beam jitter, and selective aperture geometries.

Most of the wavefront devices use high-speed digital cameras to record images, which contain information about measured wavefronts. For slope-based wavefront sensors, these digital devices limit the sampling speed of data collection. To overcome this problem, analog-only wavefront devices were developed, which use photo-sensitive diodes to record instantaneous deflection angles over sub-apertures. Examples of these devices include a Malley Probe (Gordeyev et al. 2007a), a Small-Aperture Beam Technique (SABT) sensor (Hugo & Jumper 1996) and an analog-only Shack-Hartmann wavefront sensor (Abado et al. 2010). These devices have high sampling rates (~ 100 kHz), but either measure only one-dimensional slice of the wavefront (the Malley probe) or have limited spa-

tial resolution (SABT sensor, analog-only Shack-Hartmann sensor. As a final note, Equation 13 provides a practical estimate on the minimum number of sub-apertures needed to correctly measure wavefronts, and for most subsonic flows, only a few thousand sub-apertures are sufficient for accurate measurements of OPD_{rms} .

5 AERO-OPTICAL FLOWS AND DISTORTION MECHANISMS

5.1 Turbulent Boundary Layers

The optically-aberrating effects of high-speed, turbulent boundary layers have been the subject of research since the early 1950s. The first investigation was by Liepmann (1952) and made use of the jitter angle of a thin beam of light as it traveled through the compressible boundary layer on the sides of high-speed wind tunnels as a way to quantify the crispness on Schlieren photographs. Stine & Winovich (1956) performed photometric measurements of the time-averaged radiation field at the focal plane of a receiving telescope, and this work also raised the prospect of using an optical degradation measurement as a method of inferring turbulence scales. Rose (1979) used hot-wire measurements and the linking equation (Equation 8) to estimate aero-optical aberrations caused by turbulent boundary layers, and found empirically that $OPD_{rms} \sim q\delta$, where q is the dynamic pressure and δ is the boundary-layer thickness. As reviewed by Gilbert & Otten (1982), research up until 1980 focused on the measurement of time-averaged optical distortions, either directly by optically-based methods or indirectly using fluid-mechanical measurements and the linking equation.

The development of high-temporal-resolution Malley probe and other high-speed wavefront devices in recent years allowed accurate time-space-resolved op-

tical measurements in turbulent boundary layers. Wyckham & Smits (2009) investigated the aero-optical performance of transonic and supersonic boundary layers using a two-dimensional Shack-Hartman wavefront sensor. Based on the OPD equation (Equation 5), and by assuming negligible pressure fluctuations in the boundary layer and invoking the strong Reynolds analogy (SRA) (Morkovin 1962), they proposed the scaling relation $OPD_{rms} \sim \rho M^2 \delta \sqrt{C_f} r_2^{3/2}$, where C_f is the local skin friction coefficient and r_2 is the ratio between the bulk and free-stream temperatures ($r_2 \approx 1$ at subsonic speeds). Gordeyev et al. (2011a) employed the linking equation along with the assumption of negligible pressure fluctuations and SRA to develop a model for OPD_{rms} at both subsonic and supersonic speeds. Their model takes the form $OPD_{rms} \sim \rho \delta \sqrt{C_f} F_1(M)$, where $F_1(M)$ is a function of the mean and fluctuating velocity profiles and the free-stream Mach number M ; $F_1(M) \approx M^2$ at subsonic speeds. This model was shown to correctly predict both the amplitude and the convective velocity of optically-active structures in compressible boundary layers. Both models (Wyckham & Smits 2009, Gordeyev et al. 2011a) were found to generally agree with each other up to $M = 5$.

Non-adiabatic effects with heated and cooled walls were studied by Cress (2010) and Cress et al. (2010). It was predicted and experimentally verified that proper cooling of the wall upstream of the aperture will significantly decrease aero-optical distortions. Large intermittent increases of aero-optical aberrations with subsequent drop-outs in far-field intensities have also been investigated experimentally (Gordeyev et al. 2003, Cress 2010).

All these experimental studies strongly suggest that the majority of optically-active structures in compressible boundary layers are located in the outer re-

gion of the boundary layer, moving at 0.82–0.85 times the freestream velocity. The predominant mechanism for density fluctuations in compressible boundary layers is believed to be adiabatic heating/cooling due to velocity fluctuations via strong Reynolds analogy, as pressure fluctuations inside boundary layers are much smaller than temperature fluctuations. This was also confirmed in numerical simulations (Wang & Wang 2011).

While experimental investigations have shed much light on the characteristics and scaling laws of boundary-layer aero-optics, numerical simulations have started to play a significant role in gaining physical understanding of distortion mechanisms and testing aero-optical theories and their underlying assumptions. High-fidelity approaches like DNS and well-resolved LES are ideally suited for such fundamental studies because they provide detailed spatial and temporal information about the index-of-refraction field along with the velocity field, making it possible to directly relate flow structures to optical aberrations.

Tromeur et al. (2003, 2006a, 2006b) undertook the first numerical investigation of the optical-aberrating effects of turbulent boundary layers using LES. They considered temporally and spatially evolving flat-plate boundary layers at free-stream Mach numbers of 0.9 and 2.3 and momentum-thickness Reynolds number $Re_\theta = 2917$. Converged flow and optical statistics were obtained and analyzed in the case of spatially developing boundary layers with an adiabatic wall. By comparing directly computed OPD_{rms} with that obtained using the linking equation, Equation 8, with LES density-fluctuation data, Tromeur et al. (2006a, 2006b) found significant discrepancies between the two, and consequently questioned the applicability of the linking equation to boundary-layer flows. However, it was later noted by Wang & Wang (2011) that these discrepancies were caused by

improper choice of the correlation-length definition that is inconsistent with the linking equation.

Wang & Wang (2009, 2011) performed a well-resolved LES study of optical-distortion mechanisms in a Mach 0.5, adiabatic-wall boundary layers at Reynolds numbers $Re_\theta = 875, 1770$ and 3550 . They obtained detailed statistics of fluctuating density and wavefront distortions, including the rms values, spatial and temporal correlations, and frequency spectra. Contributions from different boundary-layer regions to wavefront errors were evaluated, which shows dominance of the logarithmic layer and wake region. Consistent with the analysis of Mani et al. (2008), the effect of small-scale flow structures on optical aberrations was found to be small. The applicability of Sutton's linking equation was re-examined, and it was found that, with a definition of the density correlation-length consistent with the linking equation, the latter provides an excellent prediction of OPD_{rms} . The effect of turbulence inhomogeneity is too small to affect the validity of the linking equation. The convection velocities of the optical wavefront were computed and found to be consistent with previous experimental values.

It is well-established that turbulent boundary layers contain packets of vortical structures with a preferred angular direction (e.g. Adrian 2007, Wu & Moin 2009). They are believed to be important sources of aero-optical distortions, and therefore the boundary layer exhibits an anisotropic behavior for different elevation angles of beam propagation. This behavior was measured experimentally (Cress et al. 2008) and later observed computationally (Wang & Wang 2009, 2011). As illustrated in Figure 3, a beam is distorted more severely when it is tilted toward downstream than upstream with the same relative angle to the normal direction. This is consistent with the linking-equation prediction, Equation 8, because the

correlation length Λ is longer when the beam is aligned with the elongated vortical structures in the boundary layer (see right plot in Figure 3). Similar directional dependence of optical distortions was observed by Truman & Lee (1990) in an incompressible DNS of turbulent shear flow with uniform mean-shear rate.

Although it is generally believed that OPD_{rms} is insensitive to Reynolds number at sufficiently high Reynolds numbers, the results of Wang & Wang (2011) still exhibit a significant variation of OPD_{rms} with Reynolds number (see Figure 3), although the rate of variation is seen to decrease with increasing Reynolds number. Simulations at higher Reynolds numbers are required to allow direct, quantitative comparisons with experimental measurements, which are typically performed at much high Reynolds numbers.

5.2 Turbulent Shear Layers and Wakes

Separated turbulent shear layers are omnipresent around aero-optical devices such as turrets and laser cavities. The presence of large-scale vortical structures in shear layers was firmly established for the last 30 years or so, yet until few years ago, most models used for aero-optical aberrations in shear layers largely ignored the role of these structures, assuming that pressure fluctuations inside the shear layer are negligible and using strong Reynold analogy to compute density fluctuations. The reader is referred to Fitzgerald & Jumper (2004) for a detailed survey of different shear layer models.

Vortical structures are characterized by a strong radial pressure gradient accompanied by significant pressure fluctuations. Based on this fact, Fitzgerald & Jumper (2004) developed a physics-based numerical procedure for approximating the density field, and thus the refractive index, from a known two-dimensional

velocity-field data for total-temperature-matched shear layers. The velocity, density and pressure fields are connected by the Euler equations, and by assuming an isentropic process and using a simplified version of the energy equation and the ideal gas law, they developed a procedure for iteratively retrieving density and pressure fields based on the given velocity field. Their model, called the Weakly Compressible Model (WCM), takes into account the radial pressure gradients required to sustain the vortical flow and curved path-lines. Fitzgerald & Jumper (2004) showed that this model predicted reasonably well the experimentally-observed aero-optical aberrations for a high subsonic shear layer, when other shear-layer models failed to do so. However, as a simplified model, the accuracy of WCM is limited by its underlying assumptions. A comparison with the numerical results of a compressible shear layer obtained by Visbal (2009) using ILES with a high-order scheme shows that WCM, while correctly predicting density fluctuations inside vortical structures, is unable to predict the sharp density-gradients numerically observed in braid regions between vortical structures.

To further investigate the nature of this discrepancy, simulations for laminar mixing layers with either matched total or static temperature of the upper and lower streams were performed by Visbal (2009). It was found that when the total temperature was matched, a density interface between the two streams was apparent in the shear layer braid regions, although this effect has not yet been observed experimentally. In contrast, sharp density gradients were absent when the static temperature was matched. Despite the significant differences in the density field, the OPD distributions were found to be similar, indicating that optical distortions are dominated by compressible effects instead of density interfaces.

For transitional mixing layers, Visbal (2009) showed that optical distortions near a splitter plate are similar to those caused by laminar mixing layers and increase downstream as the mixing layer grows. The effects of forcing with either spanwise uniform or non-uniform excitations on turbulent mixing layers have been studied as well (Visbal 2008, White et al. 2010). It was shown that in general, forced mixing layers induce larger OPD, and the forcing regularizes the shear layer, confirming the experimental results of Rennie et al. (2008).

Mani et al. (2009) performed a fundamental study of optical distortions by separated shear layers and wakes using a highly accurate LES with high grid resolution. They considered a Mach 0.4 flow over a circular cylinder at Reynolds numbers $Re = 3900$ and $10,000$. They found that optical distortions by the fully developed wake was insensitive to the Reynolds number while distortions by the separated shear layers were sensitive to the Reynolds number. This finding was explained on the basis that the instability of the wake is predominantly inviscid and that the Reynolds number only affects the Kolmogorov scale which was found to be optically unimportant (Mani et al. 2008). In contrast, the instability and transition in the early separated shear layers are Reynolds-number sensitive, leading to Reynolds-number sensitivity of their optical effects.

The aero-optics of shear layers with different gases on both sides were studied by Dimotakis et al. (2001), Catrakis & Aguirre (2004), and Zubair & Catrakis (2007), to name a few. Dimotakis et al. (2001) studied subsonic shear layers at low and high Reynolds numbers with different gases on the two sides. Gases were density-matched, but had different index-of-refraction coefficients. Instantaneous snapshots of index-of-refraction fields were taken using the Rayleigh scattering technique and instantaneous wavefronts were calculated by integrating the field in

the beam-propagation direction. The large-scale structures in the shear layer were found to be the dominant source for aero-optical distortions, and a level-set model was proposed to explain observed wavefront characteristics. As pointed out by Jumper & Fitzgerald (2001), the combined aero-optical effects were from both index-of-refraction mixing and compressible turbulent mixing and, ultimately, the proposed level-set model underestimated the experimentally-measured aero-optical levels of subsonic index-of-refraction-matched compressible shear layers (Fitzgerald & Jumper 2004). Catrakis & Aguirre also used the Rayleigh scattering technique to study the aero-optical structure in dissimilar-gas mixing layers at high Reynolds numbers. They developed a new interfacial fluid thickness approach, based on tracing regions of high gradients of the index-of-refraction field, to study the physics of aero-optical distortions.

5.3 Flow over Optical Turrets

One of the most used platforms to point-and-track lasers are turrets of hemisphere-on-cylinder type. They provide a convenient way to steer-and-stay the beam in a desired direction for a transmitting station or to keep lock on the incoming beam for a receiving station. Most airborne laser-based systems, both past and present, use the turret geometry of some sort. But their less-than-ideal aerodynamic shape creates complex flow fields consisting of all major fundamental turbulent flows: boundary layers, separated shear layers, wake, necklace vortex and other large-scale vortical structures, as shown schematically in Figure 4.

Depending on the viewing direction, the laser beam will encounter one or several of these fundamental flows. Even the time-averaged flow around the turret has significant steady pressure and density gradients, causing steady-lensing ef-

fects. Flow is typically attached on the front portion of the turret with a relatively thin boundary layer, so the outgoing laser beam has mostly steady-lensing aberrations imposed on it. Flow is separated on the aft portion of the turret and, when transmitting through the separated region, the beam will experience significant unsteady aero-optical aberrations even at relatively small subsonic speeds (Gordeyev et al. 2007a, Gordeyev et al. 2007b, Vukasinovic et al. 2010, Gordeyev et al. 2010b). Aero-optical distortions in this region are predominantly caused by shear-layer vortical structures and the separation bubble formed downstream of the turret (see Figure 4). At transonic and supersonic flows, shock-induced aero-optical effects with large density gradients are added to this already complicated picture (Gordeyev & Jumper 2010).

Due to technological importance of turrets, they have been studied extensively in the 1970s and 1980s, and good reviews of research efforts during that period are presented in Gilbert & Otten (1982) and Sutton (1985). But laser systems of those days had long wavelengths (~ 10 microns), and unsteady aero-optical effects caused by turrets were found to be negligible at subsonic speeds; only steady-lensing effects were considered. The switch to shorter wavelength (~ 1 micron) laser in recent years has exacerbated the aero-optical effects, which spurred a renewed interest in aero-optics of turrets. A summary of recent efforts, including flow-control strategies to mitigate aero-optical effects around turrets, can be found in Gordeyev & Jumper (2010).

Recent experiments (Gordeyev & Jumper 2010) have shown that for subsonic flows at large Reynolds numbers, $OPD_{\text{rms}} \sim A(\text{geometry}, a/D)B(\alpha, \gamma)\rho_{\infty}M^2D$, where ρ_{∞} and M are the free-stream density and Mach number, respectively, D is the turret radius, A is a “constant” depending on the turret geometry and

the relative aperture size, a/D , and B is a function of the beam-transmitting direction, defined by window angle α and elevation angle γ shown in Figure 4. This simple scaling was found to collapse most of the experimental results available in open literature, as shown in Figure 5. The turret geometry was found to influence aero-optical aberrations. A hemispherical turret is more optically-aberrating than a hemisphere-on-cylinder turret due to increased proximity of the near-the-wall vortices to the aperture. A flat-window turret creates more aero-optical distortions compared to a conformal-window turret due to an earlier separation from the front portion of the flat-window aperture.

Numerical simulations of flow over turrets are extremely challenging due to the complex vortex structures discussed above and the wide range of flow scales associated with them. The high Reynolds numbers encountered at realistic flight or laboratory conditions make these flows out of reach by LES. In addition, simulations must cope with traditional difficulties such as the laminar-to-turbulence transition of the boundary layer and incipient separation from the turret surface. Aside from a few LES attempts (Jones & Bender 2001, Arunajatesan & Sinha 2005), which are grossly under-resolved, most recent computational efforts are based on RANS/LES hybrid approaches. Nahrstedt et al. (2008) employed the partially-averaged Navier-Stokes (PANS) method (Girimaji & Abdol-Hamid 2005) with the $k-\varepsilon$ model in a finite-volume CFD code to compute the aero-optical flow and OPD_{rms} of a 12-inch-diameter hemispherical/cylindrical turret in a wind-tunnel experiment (Gordeyev et al. 2007b) at Mach numbers ranging from 0.3 to 0.5. With a 2.7 million mesh, their results captured some aspects of the experimental measurements, but sizable discrepancies existed, and the vortical structures in the shear and wake were apparently too coherent. Ladd et al.

(2009) used DES with the two-equation $k-\omega$ SST model to compute the same flow with 3.2 million structured mesh and 10 million unstructured mesh, and obtained improved solutions. Their mean turret-surface pressure and velocity profiles at several wake stations showed reasonable agreement with experimental values, as did their OPD_{rms} over a range of elevation angles. The best resolved turret-flow simulation to date was performed by Morgan & Visbal (2010), who again considered the experimental configuration of Gordeyev et al. (2007b). Using a hybrid RANS/ILES method with a $k-\varepsilon$ model and a 6th-order compact-difference solver on a 23.6 million mesh, their simulation captured fine details of turbulence structures and many flow features observed in the experiment, but there were also significant differences in the separated region. Major discrepancies were observed between the computed OPD_{rms} values and experimental data.

Virtually all numerical simulations of turret flows to date are for turrets with a conformal window. Flows around flat-window turrets are more difficult to study both experimentally and computationally. The slope-discontinuity around the flat aperture causes a premature flow separation and creates a weak separation bubble over the aperture at some angles (Gordeyev et al. 2007a, Gordeyev et al. 2010b), leading to increased aero-optical distortions. Aside from increased geometric and flow complexity, computational expenses are higher due to the fact that a separate flow simulation is required for each viewing angle because the flow field around the turret depends on the window position.

Evidently, current computational capabilities still do not allow accurate and robust predictions of the fluctuating index-of-refraction field around a three-dimensional optical turret at realistic Reynolds numbers. Hybrid LES/RANS methods continue to offer the best practical approach in the foreseeable future,

but a number of weaknesses and outstanding issues need to be addressed. For DES methods, which treat attached boundary layers with RANS, prediction of boundary-layer transition and incipient separation from the turret surface is a significant challenge. Furthermore, the shear layer immediately after separation, which is in the optically important region, may not behave realistically without upstream turbulence. The effect of upstream turbulent fluctuations on the shear-layer instability and how to incorporate them in DES-type simulations requires further investigation.

Given the significant computational challenges for three-dimensional turrets, it would be prudent to first validate solution techniques in simpler flows that capture some crucial physical aspects of realistic turret flows. The two-dimensional cylindrical turret investigated experimentally by Gordeyev et al. (2011b) provides an excellent benchmark configuration for computational validation. Because the turret is mounted horizontally on two flat surfaces of different altitude, the flow upstream of the turret is a flat-plate turbulent boundary layer, which can be easily characterized and realistic turbulent inflow can be fed into the simulation (Wang & Wang 2009). This configuration has been employed in a number of recent LES investigations (Morgan & Visbal 2010, Wang & Wang 2009, Wang et al. 2010).

6 CONCLUDING REMARKS

Aero-optics is an interdisciplinary area that has seen a renewed interest and significant growth over the past decade. At the core of aero-optical phenomena is compressible turbulence, whose accurate prediction in a practical aero-optical environment over optically active flow scales remains a significant challenge. This

review is focused on the fundamental understanding and prediction of aero-optics, and related numerical and experimental techniques. Given the diverse nature of the field and space limitation, the contents in this article are necessarily selective; they are by no means reflective of the relative level of research activities or accomplishments. Computational techniques and their applications to aero-optical problems are afforded more coverage considering the growing role of computations and their future promise.

The discussions presented in this paper are mostly on the aero-optical effects of subsonic flows. The presence of shock waves and shock-turbulence interaction in a supersonic flow exacerbates aero-optical effects and gives rise to additional computational and experimental challenges, which are not discussed here. Wavefront sensors and data reduction algorithms are only briefly mentioned, but they are the most critical part in collecting accurate aero-optical measurements.

Another important part of aero-optics research not covered in the present article is mitigation strategies. The goal of aero-optical mitigations is to reduce the overall distortions of an optical beam, which can be achieved through a variety of flow control and/or adaptive optic techniques. Passive control devices placed in front of an optical turret have shown promise (Gordeyev et al. 2010a), and active flow control using pulsating micro-jets has effectively reduced aero-optical distortions around turrets (Vukasinovic et al. 2010). Although adaptive optics alone currently only works for low-frequency aberrations typical of atmospheric turbulence, progress has been made in extending it to high-frequency aero-optics. One promising technique, which has been demonstrated in a compressible shear layer (Rennie et al. 2008), involves a combination of adaptive optics with flow control. By first regularizing the flow using active flow control, the aberrations become

predictable and can be corrected by a deformable mirror without instantaneous wavefront measurements.

In the development of mitigation techniques for optical systems, fundamental understanding of aero-optical mechanisms gained through physical and numerical experiments has played and will continue to play an essential role. Further advances in experimental and computational techniques leading to accurate predictive tools are much needed in order to accelerate the development of practical airborne laser systems.

ACKNOWLEDGMENTS

The authors acknowledge support from the Air Force Office of Scientific Research, the High Energy Laser Joint Technology Office, and the Air Force Research Laboratory for research in this area. We would like to thank Eric Jumper and colleagues in the Aero-Optics Group at the University of Notre Dame and Parviz Moin of Stanford University for many fruitful discussions.

LITERATURE CITED

- Abado S, Gordeyev S, Jumper E. 2010. Two-dimensional high-bandwidth Shack-Hartmann wavefront sensor: design guidelines and evaluation testing. *Opt. Eng.* 49(6):064403.
- Adrian RJ. 2007. Hairpin vortex organization in wall turbulence. *Phys. Fluids* 19(4):1-16.
- Arunajatesan S, Sinha N. 2005. Analysis of line of sight effects in distortions of laser beams propagating through a turbulent turret flow field. AIAA Pap. 2005-1081
- Blanchard P, Fisher D, Woods SC, Greenaway AH. 2000. Phase-diversity wave-front sensing with a distorted diffraction grating. *Appl. Optics*, 39(35):6649-55
- Born M, Wolf, E. 2002. *Principles of Optics*, 7th ed. Cambridge: Cambridge Univ. Press. 952

pp.

- Cassady, PE, Birch, SF, Terry, PJ. 1989. Aero-optical analysis of compressible flow over an open cavity. *AIAA J.* 27(6):758–62
- Catrakis HJ, Aguirre RC. 2004. New interfacial fluid thickness approach in aero-optics with applications to compressible turbulence. *AIAA J.* 43(10):1973–81
- Chernov LA. 1960. *Wave Propagation in a Random Medium*. New York: McGraw-Hill. 168 pp.
- Childs RE. 1993 Prediction and control of turbulent aero-optical distortion using large eddy simulation. AIAA Pap. 93-2670
- Coles WmA, Filice JP, Frehlich RG, Yadlowsky M. 1995. Simulation of wave propagation in three-dimensional random media. *Appl. Optics* 34(12):2089–101
- Cress J, Gordeyev S, Post M, Jumper EJ. 2008. Aero-optical measurements in a turbulent, subsonic boundary layer at different elevation angles. AIAA Pap. 2008-4214
- Cress JA. 2010. Optical aberrations caused by coherent structures in a subsonic, compressible, turbulent boundary layer. *Ph.D. Thesis*, Univ. of Notre Dame, Notre Dame, IN
- Cress J, Gordeyev S, Jumper E. 2010. Aero-optical measurements in a heated, subsonic, turbulent boundary layer. AIAA Pap. 2010-0434
- Dimotakis PE, Catrakis HJ, Fourguette DC. 2001. Flow structure and optical beam propagation in high-Reynolds number gas-phase shear layer and jets. *J. Fluid Mech.* 433:105–34
- Fitzgerald EJ, Jumper EJ. 2002. Scaling aero-optic aberrations produced by high-subsonic-Mach shear layers. *AIAA J.* 40(7):1373–81
- Fitzgerald EJ, Jumper EJ. 2004. The optical distortion mechanism in a nearly incompressible free shear layer. *J. Fluid Mech.* 512:153–89
- Frehlich R. 2000. Simulation of laser propagation in a turbulent atmosphere. *Appl. Optics* 39(3):393–97
- Germano M, Piomelli U, Moin P, Cabot WH. 1991. A dynamic subgrid-scale eddy viscosity model. *Phys. Fluids A* 3(7):1760–65
- Gilbert KG, Otten LJ. eds. 1982. *Aero-Optical Phenomena, Progress in Astronautics and Aeronautics, Vol. 80*. New York: AIAA. 412 pp.
- Girimaji SS, Abdol-Hamid KS. 2005 Partially-averaged Navier-Stokes model for turbulence: implementation and validation. AIAA Pap. 2005-502

- Goodman JW. 2004. *Introduction to Fourier Optics*, 3rd ed. Roberts & Company. 466 pp.
- Gordeyev S, Jumper E, Ng T, Cain A. 2003. Aero-optical characteristics of compressible, subsonic turbulent boundary layer. AIAA Pap. 2003-3606
- Gordeyev S, Hayden T, Jumper E. 2007a Aero-optical and flow measurements over a flat-windowed turret. *AIAA J.* 45(2):347–57
- Gordeyev S, Post M, MacLaughlin J, Cenicerros J, Jumper E. 2007b Aero-optical environment around a conformal-window turret. *AIAA J.* 45(7):1514–24
- Gordeyev S, Jumper EJ. 2010. Fluid dynamics and aero-optics of turrets. *Prog. Aerospace Sci.* 46:388–400
- Gordeyev S, Cress JA, Smith A, Jumper EJ. 2010a. Improvement in optical environment over turrets with flat window using passive flow control. AIAA Pap. 2010-4492
- Gordeyev S, Jumper E, Vukasinovic B, Glezer A, Kibens V. 2010b. Hybrid flow control of a turret wake, part II: aero-optical effects. AIAA Pap. 2010-0438
- Gordeyev S, Jumper EJ, Hayden T. 2011a. Aero-Optics of Supersonic Boundary Layers. AIAA Pap. 2011-1325
- Gordeyev S, Cress JA, Jumper EJ, Cain AB. 2011b. Aero-optical environment around a cylindrical turret with a flat window. *AIAA J.* 49(2):308–15
- Hardy JW. 1998. *Adaptive Optics for Astronomical Telescopes*. Oxford: Oxford Univ. Press. 438 pp.
- Havener G. 1992. Optical wave front variance: a study on analytic models in use today. AIAA Pap. 92-0654
- Hugo, RJ, Jumper EJ, 1996. Experimental measurement of a time-varying optical path difference by the small-aperture beam technique. *Appl. Optics* 35(22):4436-47
- Hugo RJ, Jumper EJ. 2000. Applicability of the aero-optic linking equation to a highly coherent, transitional shear layer. *Appl. Optics* 39(24):4392–401
- Jones MI, Bender EE. 2001 CFD-based computer simulation of optical turbulence through aircraft flowfields and wakes. AIAA Pap. 2001-2798
- Jumper EJ, Fitzgerald EJ. 2001. Recent advances in aero-optics. *Prog. Aerospace Sci.* 37:299–339
- Ladd J, Mani M, Bower W. 2009 Validation of aerodynamic and optical computations for the

- flow about a cylindrical/hemispherical turret. AIAA Pap. 2009-4118
- Liepmann HW. 1952. Deflection and diffusion of a light ray passing through a boundary layer. *Tech. Rep. SM-14397*, Douglas Aircraft Company, Santa Monica Division, Santa Monica, CA
- Lilly DK. 1992. A proposed modification of the Germano subgrid scale closure method. *Phys. Fluids A* 4(3):633–35
- Lloyd-Hart M. 2003. Taking the twinkle out of starlight. *IEEE Spectrum* 40(12):22–29
- Mahajan VN 1982. Strehl ratio for primary aberrations: some analytical results for circular and annular pupils. *J. Opt. Soc. Am.* 72(9):1258–66
- Mahajan VN 1983. Strehl ratio for primary aberrations in terms of their aberration variance *J. Opt. Soc. Am.* 73(6):860–61
- Mani A, Wang M, Moin P. 2006. Statistical description of free-space propagation of highly aberrated optical beams. *J. Opt. Soc. Am. A* 23(12):3027–35
- Mani A, Wang M, Moin P. 2008. Resolution requirements for aero-optical simulations. *J. Comput. Phys.* 227:9008–20
- Mani A, Moin P, Wang M. 2009. Computational study of optical distortions by separated shear layers and turbulent wakes. *J. Fluid Mech.* 625:273–98
- Maréchal A. 1947. Étude des effets combinés de la diffraction et des aberrations géométriques sur l'image d'un point lumineux *Rev. Opt. Theor. Instrum.* 26:257–77
- Moin P, Squires KD, Cabot WH, Lee S. 1991. A dynamic subgrid-scale model for compressible turbulence and scalar transport. *Phys. Fluids A* 3(11):2746–57
- Moin P, Mahesh K. 1998. Direct numerical simulation: a tool in turbulence research. *Annu. Rev. Fluid Mech.* 30:539-78
- Monin AS, Yaglom, AM. 1975. *Statistical Fluid Mechanics: Mechanics of Turbulence, Vol. II*, ed. JL Lumley, Chap. 9, Cambridge, Mass: MIT Press. 886 pp.
- Morgan PE, Visbal MR. 2010. Large eddy simulation of flow over a flat window cylindrical turret with passive flow control. AIAA Pap. 2010-916
- Morkivin MV. 1962. Effects of compressibility on turbulent flows. In *Mechanique de la Turbulence*, ed. A. Favre, CNRS, pp. 367–380. Paris, France
- Nahrstedt D, Hsia Y-C, Jumper E, Gordeyev S, Ceniceros J, Weaver L, DeSandre L, McLaughlin T. 2008. Wind tunnel validation of computational fluid dynamics-based aero-optics model.

- Proc. IMechE Part G: J. Aerosp. Eng.* 223(G4):393-406
- Piomelli U, Balaras E. 2002. Wall-layer models for large-eddy simulations. *Ann. Rev. Fluid Mech.* 34:349–74
- Pond JE, Sutton GW. 2006 Aero-optic performance of an aircraft forward-facing optical turret. *J. Aircraft* 43(3):600–07
- Porter C, Gordeyev S, Zenk M, Jumper E. 2011. Flight measurements of aero-optical distortions from a flat-windowed turret on the airborne aero-optics laboratory (AAOL). To be presented at 42nd AIAA Plasmadynamics and Lasers Conference, Hawaii, June 2011.
- Rennie RM, Duffin DA, Jumper EJ, 2008. Characterization and aero-optic correction of a forced two-dimensional weakly compressible shear layer. *AIAA J.* 46(11):2787–95.
- Rose WC. 1979. Measurements of aerodynamic parameters affecting optical performance. *Air Force Weapons Laboratory Final Report AFWL-TR-78-191*, Kirtland AFB, NM
- Ross TS. 2009. Limitations and applicability of the Maréchal approximation. *Appl. Optics* 48(10):1812–18
- Sasiela RJ. 2007. *Electromagnetic Wave Propagation in Turbulence: Evaluation and Application of Mellin Transforms*. 2nd ed. Bellingham, WA: SPIE Press. 369 pp.
- Sinha N, Arunajatesan S, Seiner JM, Ukeiley LS. 2004. Large-eddy simulations of aero-optic flow fields and control application. AIAA Pap. 2004-2448
- Smagorinsky J. 1963. General circulation experiments with the primitive equations. I. The basic experiment. *Mon. Weath. Rev.* 91:99–164
- Smith RR, Truman CR, Masson BS. 1990. Prediction of optical phase degradation using a turbulent transport equation for the variance of index-of-refraction fluctuations. AIAA Pap. 90-0250
- Spalart PR. 2009. Detached-eddy simulation. *Annu. Rev. Fluid Mech.* 41:181-202
- Stine HA, Winovich W. 1956 Light diffusion through high-speed turbulent boundary layers. *Research Memorandum A56B21*, NACA, Washington
- Steinmetz WJ. 1982. Second moments of optical degradation due to a thin turbulent layer. In *Aero-Optical Phenomena, Progress in Astronautics and Aeronautics, Vol. 80*, ed. KG Gilbert, LJ Otten, pp. 78–100. New York: AIAA.
- Sutton GW. 1969. Effects of turbulent fluctuations in an optically active fluid medium. *AIAA*

- J.* 7(9):1737-43
- Sutton GW. 1985. Aero-optical foundations and applications. *AIAA J.* 23(10):1525–37
- Tatarski VI. 1961. *Wave Propagation in a Turbulent Medium*. New York: McGraw-Hill. 285 pp.
- Tromeur E, Garnier E, Sagaut P, Basdevant C. 2003. Large eddy simulations of aero-optical effects in a turbulent boundary layer. *J. Turbul.* 4(005):1–22
- Tromeur E, Garnier E, Sagaut P. 2006a. Large eddy simulation of aero-optical effects in a spatially developing turbulent boundary layer. *J. Turbul.* 7(1):1–28
- Tromeur E, Garnier E, Sagaut P. 2006b. Analysis of the Sutton model for aero-optical properties of compressible boundary layers. *J. Fluids Eng.* 128:239–46
- Truman CR, Lee MJ. 1990. Effects of organized turbulence structures on the phase distortion in a coherent optical beam propagating through a turbulent shear flow. *Phys. Fluids A* 2(5):851–57
- Truman CR. 1992. The influence of turbulent structure on optical phase distortion through turbulent shear flows. AIAA Pap. 92-2817
- Tsai YP, Christiansen WH. 1990. Two-dimensional numerical simulation of shear-layer optics. *AIAA J.* 28(12):2092–97
- Tyson RK. 1997. *Principles of Adaptive Optics*. 2th ed. Boston: Academic Press. 345 pp.
- Tyson RK, ed. 2000. *Adaptive Optics Engineering Handbook*. New York: Marcel Dekker. 339 pp.
- Visbal MR. 2008. Effect of flow excitation on aero-optical aberration. AIAA Pap. 2008-1074
- Visbal MR. 2009. Numerical simulation of aero-optical aberration through weakly-compressible shear layers. AIAA Pap. 2009-4298
- Vukasinovic B, Glezer A, Gordeyev S, Jumper E, Kibens V. 2010 Fluidic control of a turret wake: aerodynamic and aero-optical effects. *AIAA J.* 48(8):1686–99
- Wang M, Moin P. 2002. Dynamic wall modeling for large-eddy simulation of complex turbulent flows. *Phys. Fluids* 14(7):2043–51
- Wang K, Wang M. 2009. Numerical simulation of aero-optical distortions by a turbulent boundary layer and separated shear layer. AIAA Pap. 2009-4223
- Wang K, Wang M, Gordeyev S, Jumper E. 2010. Computation of aero-optical distortions over a cylindrical turret with passive flow control. AIAA Pap. 2010-4498

- Wang K, Wang M. 2011. Aero-optical distortions by subsonic turbulent boundary layers. Submitted
- White MD. 2010. High-order parabolic beam approximation for aero-optics. *J. Comput. Phys.* 229:5465–85
- White MD, Morgan PE, Visbal MR. 2010. High-fidelity aero-optical analysis. AIAA Pap. 2010-433
- White MD, Visbal MR. 2010. High-fidelity analysis of aero-optical interaction with compressible boundary layers. AIAA Pap. 2010-4496
- Wolters DJ. 1973. Aerodynamic effects on airborne optical systems. *Tech. Rep. MDC A2582*, McDonnell Douglas Corporation, St. Louis, MO
- Wyckham CM, Smits AJ. 2009. Aero-optic distortion in transonic and hypersonic turbulent boundary layers. *AIAA J.* 47(9):2158–68
- Wolfe WL, Zizzis GJ. 1978. *The Infrared Handbook*. Office of Naval Research, Department of the Navy.
- Wu X. 2009. Direct numerical simulation of turbulence in a nominally-zero-pressure-gradient flat-plate boundary layer. *J. Fluid Mech.* 630:5–41
- Zubair FR, Catrakis HJ. 2007 Aero-optical resolution robustness in turbulent separated shear layers at large Reynolds numbers. *AIAA J.* 45(11):2721–28

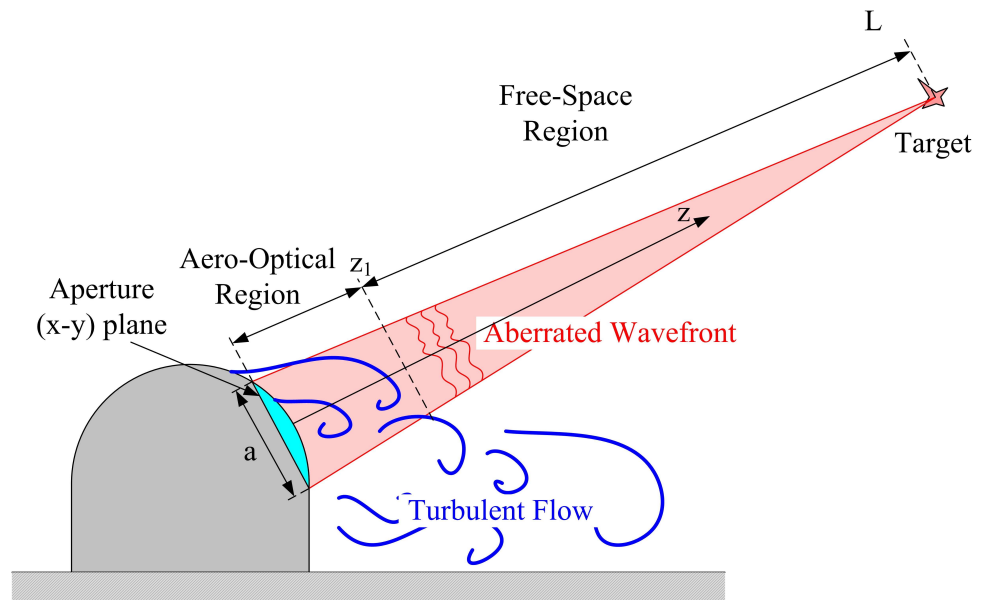


Figure 1: Schematic of the aero-optics problem.

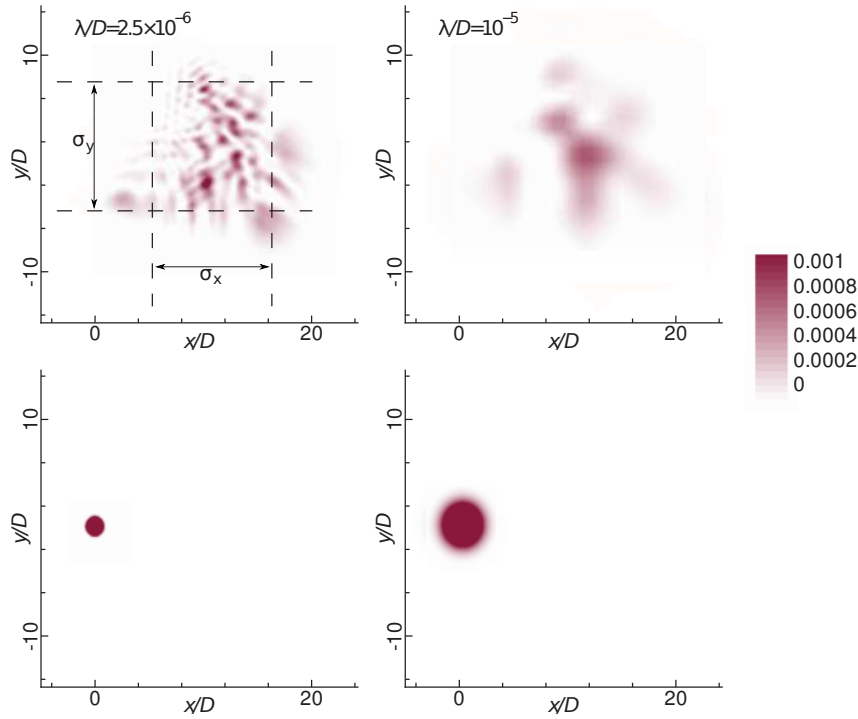


Figure 2: Instantaneous far-field optical irradiance for Gaussian beams through the wake of a circular cylinder of diameter D at a distance of $10^5 D$ for two optical wavelengths. The top plots show the distorted beams, and the bottom plots show the undistorted, diffraction limited beams. The aperture diameter is $a = 0.3D$. The peak dimensionless intensity (relative to the aperture value) for the undistorted beams are 0.074 and 0.005 for $\lambda/D = 2.5 \times 10^{-6}$ and 10^{-5} , respectively. The results are obtained using LES at free-stream Mach number $M = 0.4$ and Reynolds number $Re_D = 3900$ (Mani et al. 2009).

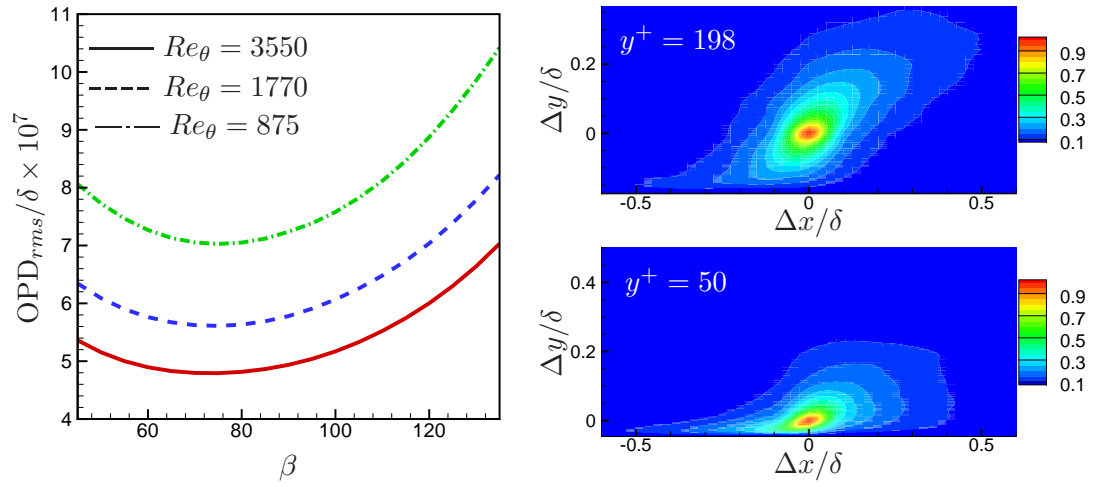


Figure 3: Left: OPD_{rms} variation with elevation angle (measured from upstream wall) for an optical beam passing through a Mach 0.5 turbulent boundary layer at three different Reynolds numbers. The aperture size is 7δ in streamwise (x) and 2.4δ in spanwise (z) directions. Right: two-point spatial correlations of density fluctuations in the x - y plane at two wall-normal locations for $Re_\theta = 3550$. The results are obtained from LES (Wang & Wang 2011).

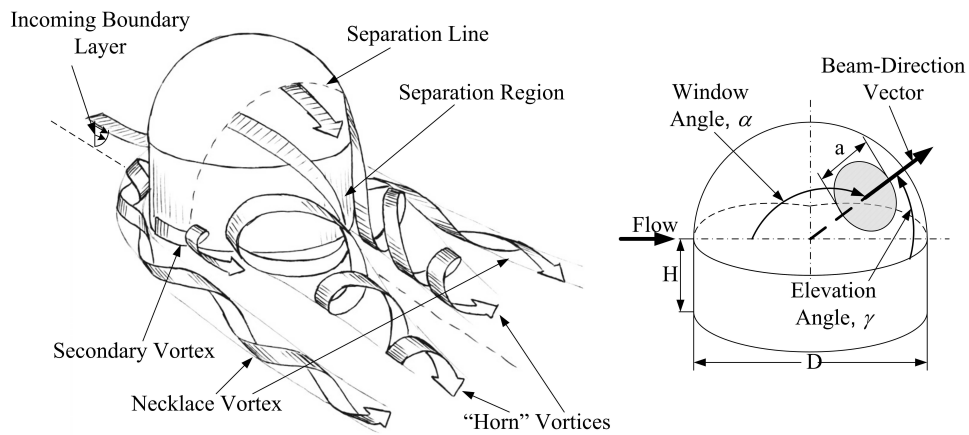


Figure 4: Flow topology around an optical turret and measurement coordinates, from Gordeyev & Jumper (2010).

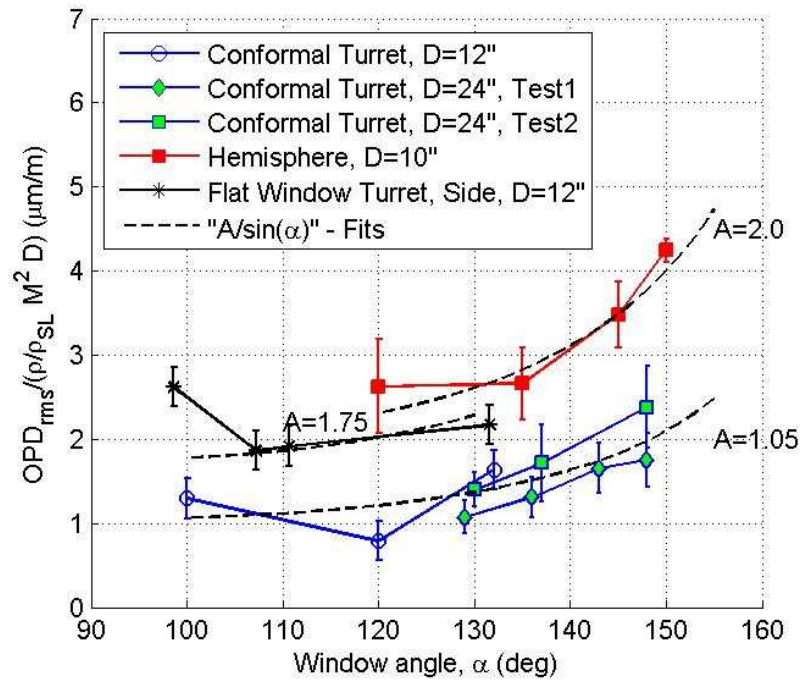


Figure 5: Normalized levels of aero-optical distortions induced by turret flows measured for different viewing angles and turret geometries (Gordeyev & Jumper 2010).